Electronic supplementary information for:

Maximizing power generation from ambient stray magnetic fields around smart infrastructures enabling self-powered wireless devices

Hyeon Lee,[a] Rammohan Sriramdas,[a,c] Prashant Kumer,[a] Mohan Sanghadasa,[b] Min Gyu Kang,*[a,c] and Shashank Priya*[a,c]

[a.] *Center for Energy Harvesting and Systems (CHEMS), Virginia Tech, Blacksburg, VA 24061, USA. Email: mgkang@psu.edu, sup103@psu.edu*
[b.] *Aviation and Missile Center, U.S. Army Combat Capabilities Development Command, Redstone Arsenal, AL 35898*
[c.] *Department of Materials Science and Engineering, Pennsylvania State University, University Park, PA 16802, USA*

Contents

This file includes;

Tables

Figures

Fig. S13. Measured and modeled output voltages as a function of load resistance and applied AC magnetic field.

Fig. S14. Modeled open circuit voltage output of the ME coupled MME and MME generators as a function of applied AC magnetic field.

Fig. S15. (a) Average power output of M4 generator under 300 μT AC magnetic field. (b) Impedance of the M4 generator as a function of frequency.

Fig. S16. Average power of the ME coupled MME generators as a function of load resistance under (a) 50 μT (b) 100 μT (c) 300 μT (d) 500 μT.

Fig. S17. Powering LED arrays (a) Electric circuit design for powering the LED arrays. (b) Experimental setup (c) The M4 generator turns on 120, 210, and 640 LEDs under 50 μT, 100 μT, and 300 μT. The LEDs are continuously lighted without charging a capacitor.

Fig. S18. (a) Electric circuit design for charging capacitors. (b) Experimental setup.

Fig. S19. Schematic description of layered configuration of MME generator.

Other supplementary information for this manuscript

Movie S1. Powering LED arrays under various AC magnetic field strength.

Movie S2. Powering a small incandescent light bulb using charged power in a 1 F supercapacitor.

Movie S3. Powering 180 LED arrays at 10 cm away from the space heater.

Movie S4. Powering a digital clock at 20 cm away from the space heater.

Movie S5. Powering an integrated sensor and wireless communication system at 4.5 cm away from the space heater.

S1. Fabrication and characterization of magnetoelectric (ME) coupled magneto-mechano-electric (MME) generators

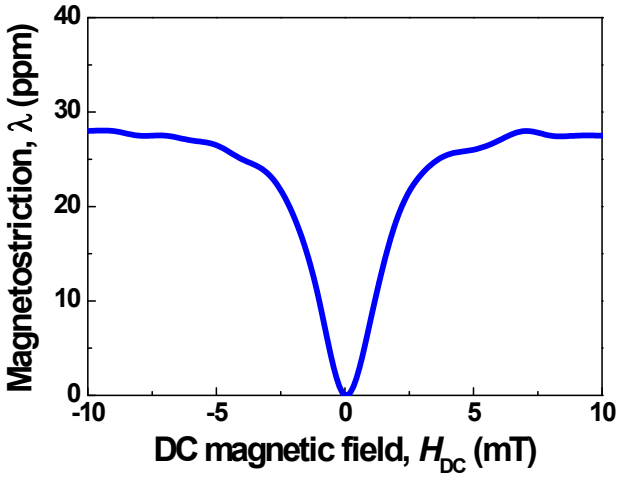

Fig. S1. Magnetostriction curve of a pristine amorphous $Fe_{85}B_5Si_{10}$ alloy sheet.

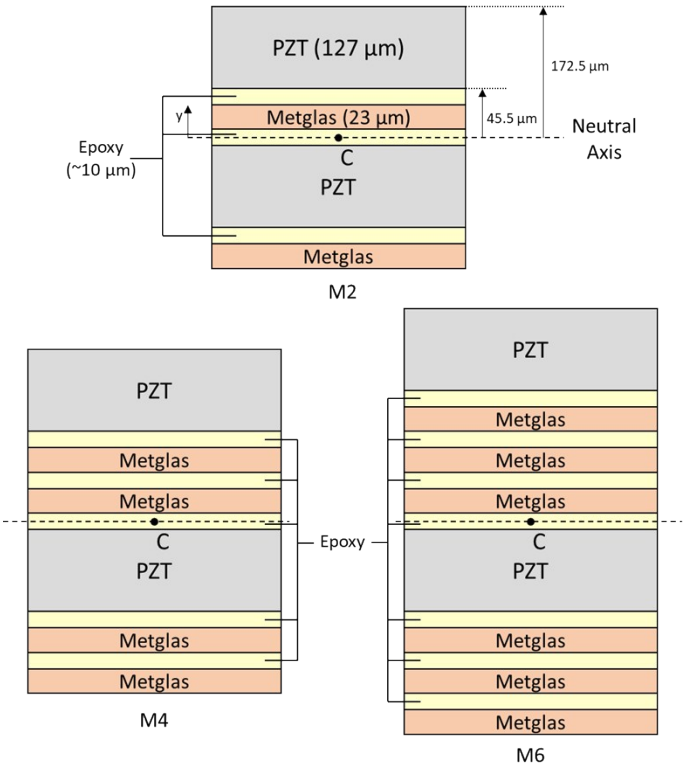

Fig. S2. Geometries of the three different ME coupled MME generators demonstrated in this study.

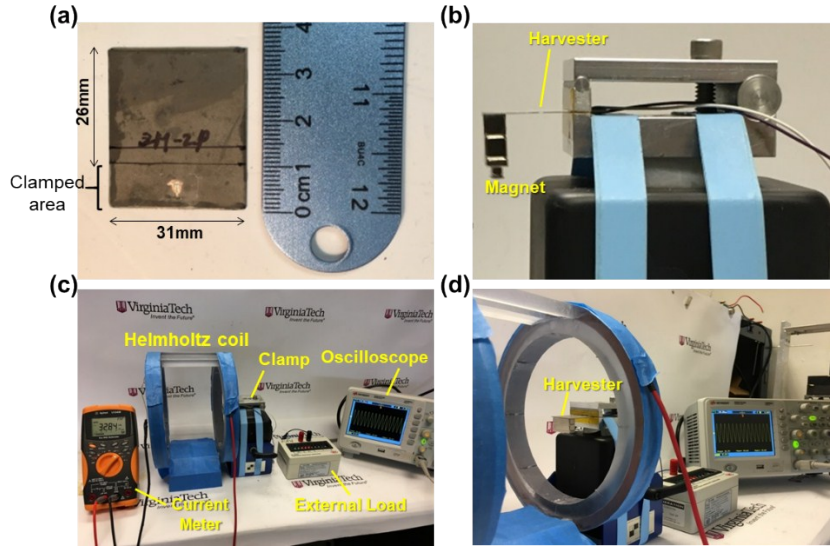

Fig, S3. Experimental setup for magnetic energy harvesting. (a) Photograph of the MME generator. (b) The MME generator was tightly clamped using a non-magnetic aluminum clamp. (c) Experimental setup to measure voltage and power output from the MME generators under homogeneous AC magnetic fields. (d) The MME generators were laterally placed along the magnetic field direction.

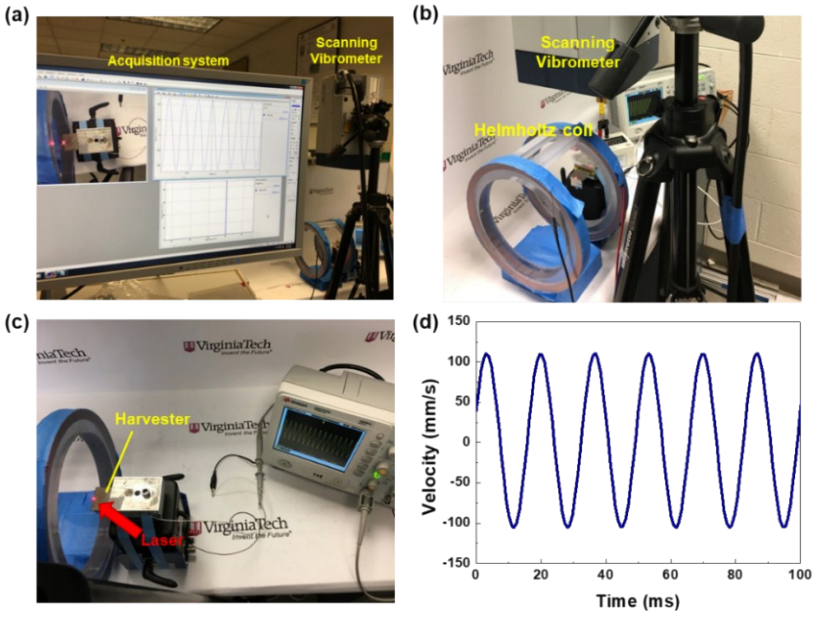

Fig. S4. Acceleration measurement setup. (a) A scanning vibrometer was used to measure the tip acceleration of the MME generators, (b-c) while the MME generators produce power under magnetic fields. (d) An example of raw tip velocity data acquired from M4 generator at 100 μT.

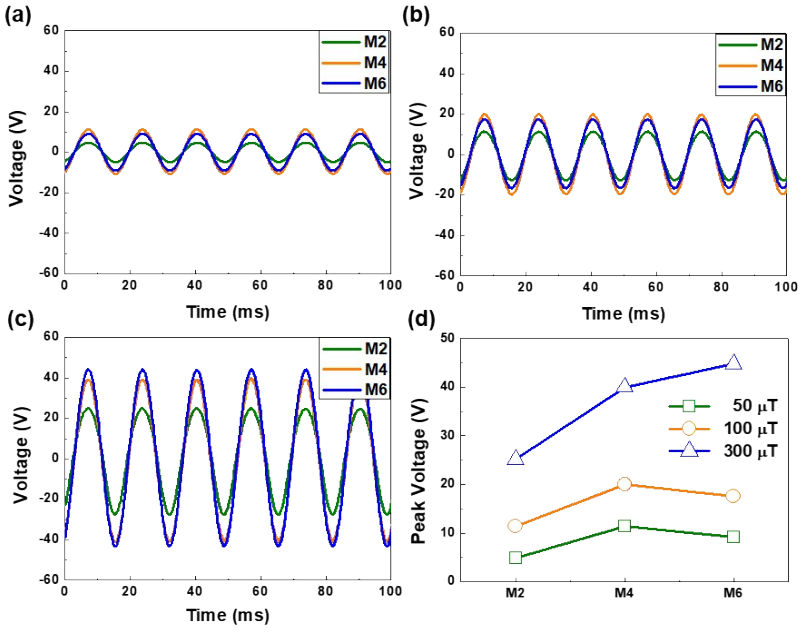

Fig. S5. Output voltages of the ME coupled MME generators under various applied AC magnetic field. Output waveforms of the MME generators under (a) 50 μT, (b) 100 μT, and (c) 300 μT magnetic fields. (d) Peak voltage outputs of the MME generators under various applied AC magnetic fields.

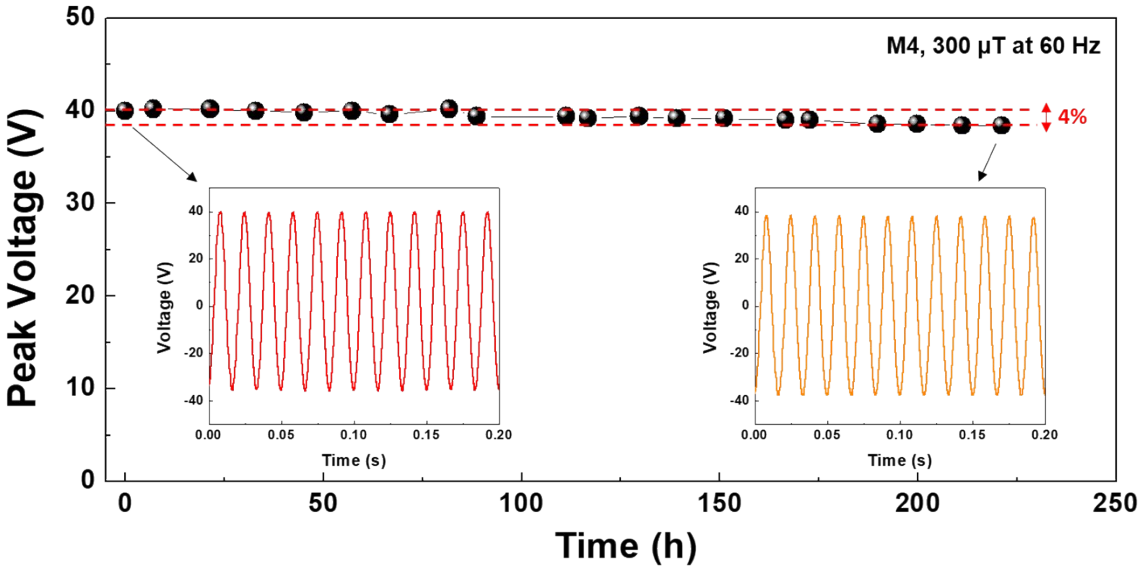

Fig. S6. Time dependent peak voltage generated from M4 generator under 300 μT. The test was performed over ten days continuously. After 10 day, the M4 generator showed only 4% in output voltage.

S2. Modeling: magneto-mechacally induced stress and generated piezoelectric potential

To investigate the relationship between the flexural rigidity of the MME generator, applied stress from the magneto-mechanical vibration, and generated piezoelectric potential, a finite-element modeling (FEM) was performed using COMSOL Multiphysics® modeling software. The piezoelectric module with frequency domain study was used and exactly same geometry of the MME generator was used in the modeling condition as shown in Fig S6. The material parameters, which are acquired from the vendor's materials specification (Table S1), were reflected to the modeling. To obtain actual piezoelectric potential value, capacitance and dielectric loss factor at 60 Hz (Fig. S7) were reflected with following equation,[1]

$$g_{31}^{*} = g_{31}\frac{1}{tan\delta^{'} + tan\theta^{'} + \frac{C - C_f}{C_f}} \quad \text{(S1)}$$

where, g_{31}^{*}, g_{31}, $tan\delta^{'}$, $tan\theta^{'}$, C_f, and C are effective piezoelectric voltage coefficient, piezoelectric voltage coefficient, intensive dielectric loss, piezoelectric loss, capacitance at 60 Hz, and capacitance at 1 kHz, respectively. As an input force, measured acceleration value produced by magneto-mechanical vibration (Fig. 2a in main manuscript) is applied at tip end. Out-of plane displacement (z-axis), in-plane stress (x-axis), in-plane strain (x-axis), and out-of-plane piezoelectric potential (z-axis) are obtained at 60 Hz resonance frequency.

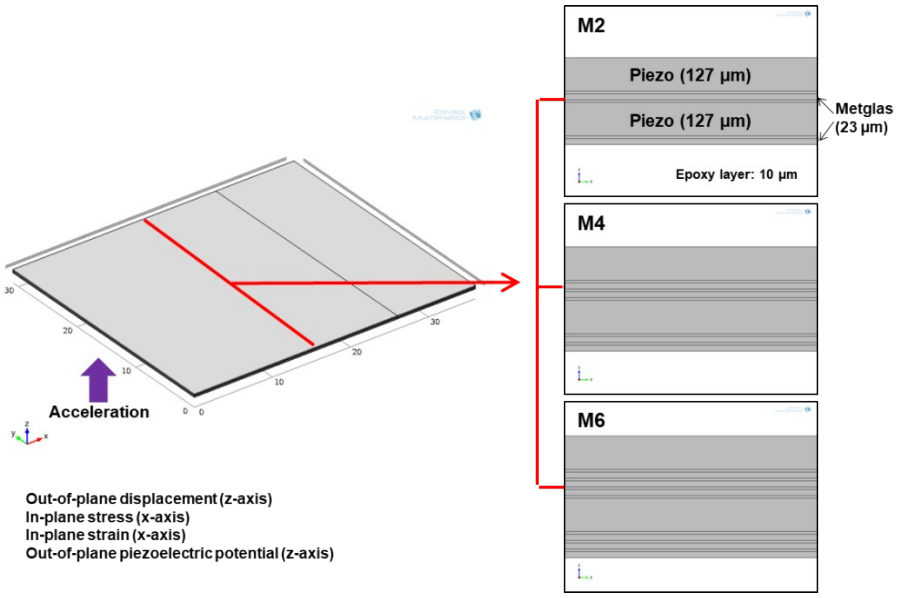

Fig. S7. Modeling condition for stress and piezoelectric potential analysis.

Table S1. Material parameters for the modeling.

		PZT 5A (PSI-5A4E)	**Metglas (2605SA)**	**Epoxy (DP-460)**
Density (kg/m^3)		7800	7180	1250
Poison Ratio		-	0.3	0.35
Young's Modulus (GPa)		-	100	7.8
d_{33} (pC/N)		390	-	-
d_{31} (pC/N)		-190	-	-
s^E_{11} ($\times 10^{-12}$ m^2/N)		16.4	-	-
s^E_{12} ($\times 10^{-12}$ m^2/N)		-5.74	-	-
s^E_{13} ($\times 10^{-12}$ m^2/N)		-7.22	-	-
s^E_{33} ($\times 10^{-12}$ m^2/N)		18.8	-	-
s^E_{55} ($\times 10^{-12}$ m^2/N)		47.5	-	-
s^E_{66} ($\times 10^{-12}$ m^2/N)		44.3	-	-
Dielectric Permittivity (ε^T)	@ 60 Hz	2240	-	-
	@ 1 kHz	2150	-	-
Dielectric Loss ($tan\delta$)	@ 60 Hz	0.248	-	-
	@ 1 kHz	0.042	-	-
Q_m		80	-	-

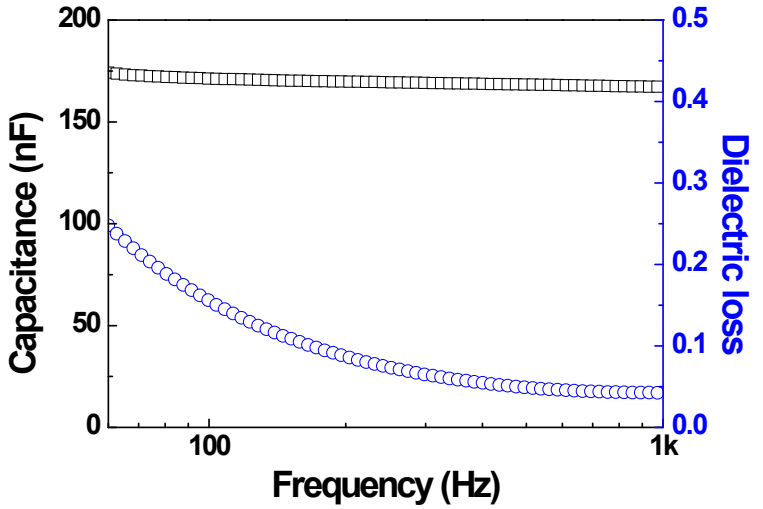

Fig. S8. Frequency dependent dielectric properties of a single piezoelectric sheet.

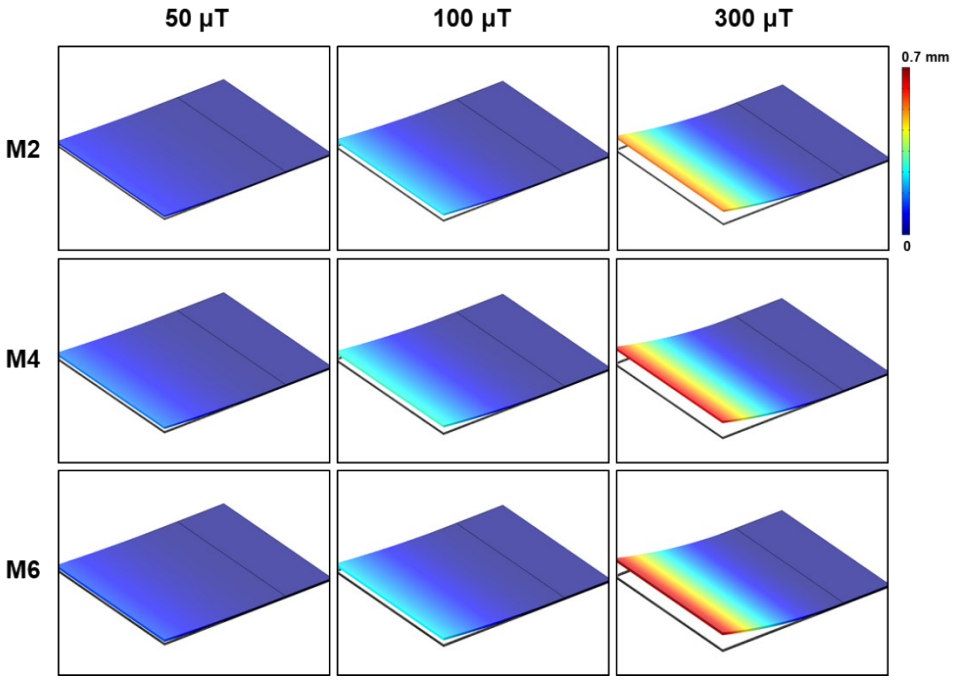

Fig. S9. Out-of-plane displacement profiles in the MME generators under various applied magnetic fields.

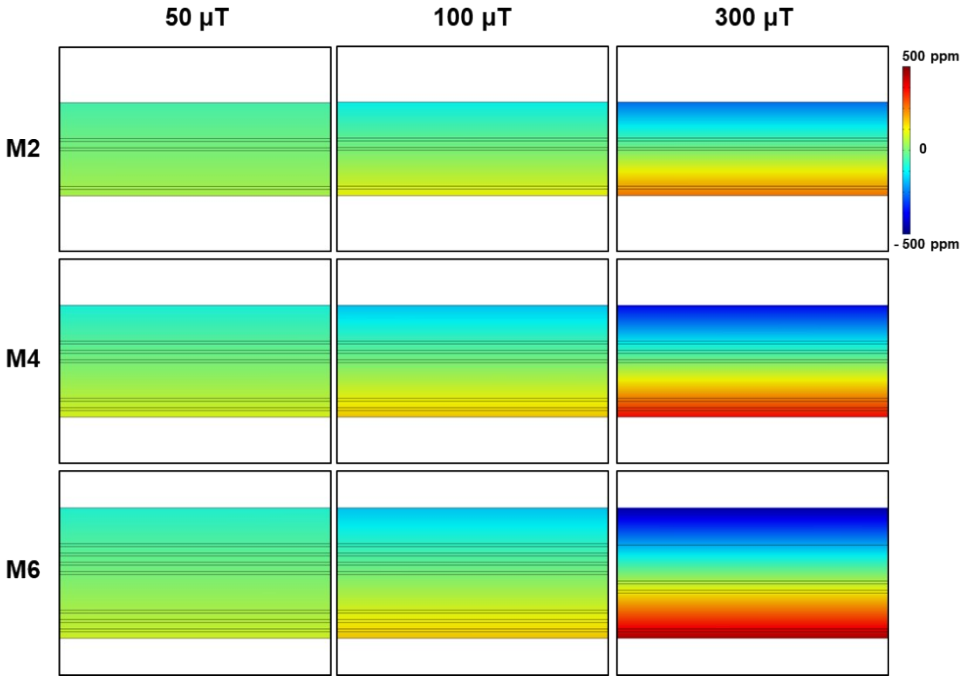

Fig. S10. In-plane strain profiles in the MME generators under various applied magnetic fields.

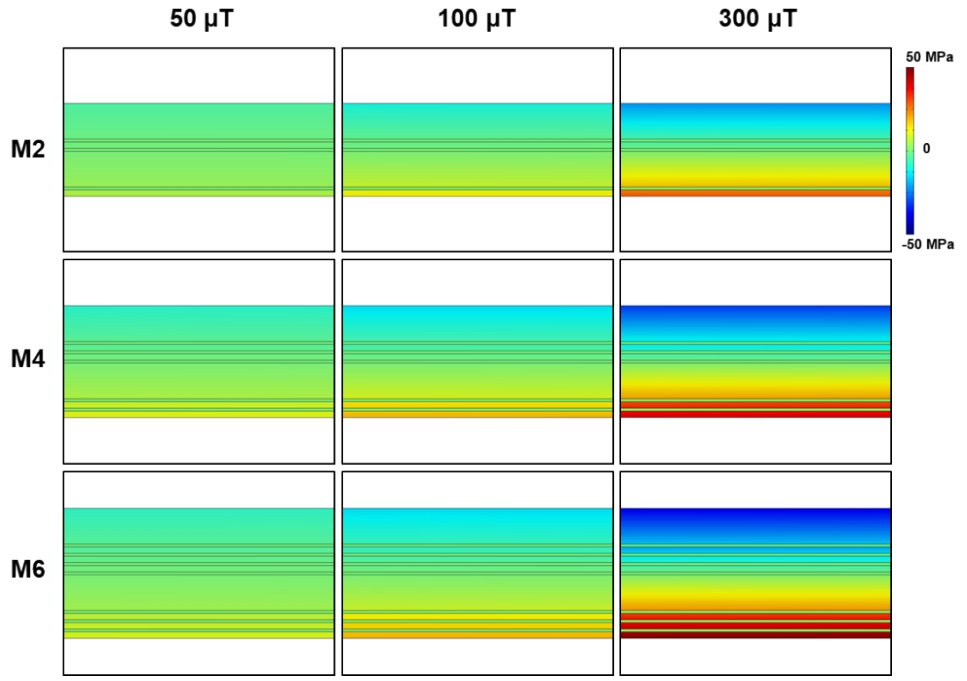

Fig. S11. In-plane stress profiles in the MME generators under various applied magnetic fields.

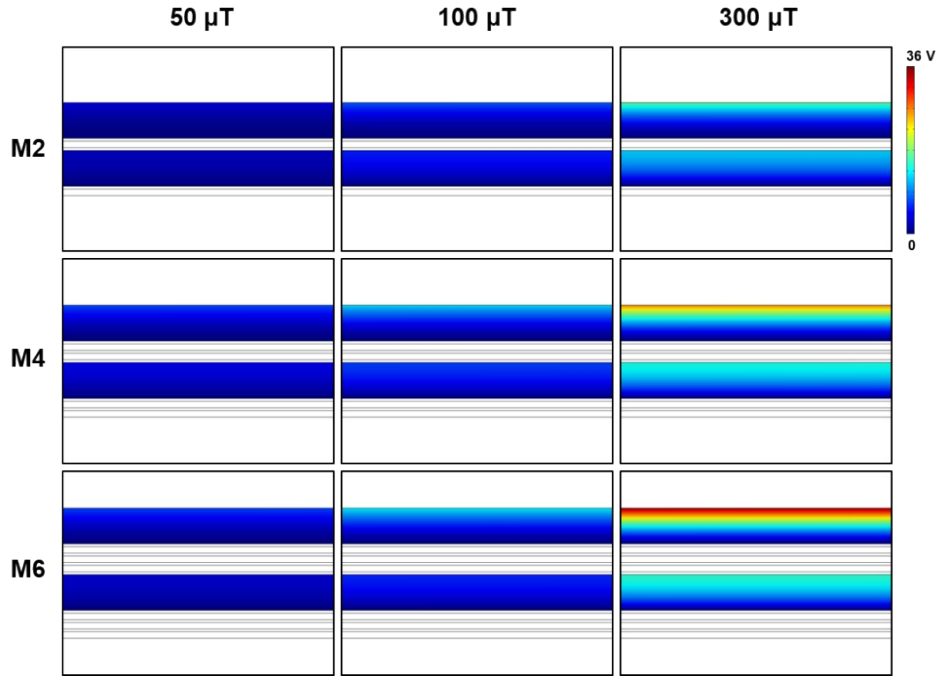

Fig. S12. Out-of-plane piezoelectric potential profiles in the MME generators under various applied magnetic fields.

Table S2. Summary of measured tip acceleration, generated peak voltage, and modeled peak voltage of the generators under various magnetic fields.

		M2	**M4**	**M6**
Tip acceleration (m/s^2)	@ 50 μT	15.24	24.12	18.8
	@ 100 μT	34.37	41.82	36.03
	@ 300 μT	75.69	90.81	95.47
Peak voltage (experimental) (V)	@ 50 μT	4.8	11.4	9.2
	@ 100 μT	11.4	20.2	17.6
	@ 300 μT	25.2	40.0	44.8
Peak voltage (modeling) (V)	@ 50 μT	5.84	11.03	9.95
	@ 100 μT	13.18	19.12	19.1
	@ 300 μT	29.05	41.51	50.6

Table S3. Summary of modeling results. Note that Piezo1 and Piezo2 are top and bottom piezoelectric sheets, respectively. The stress and strain values are collected at the center of each piezoelectric sheet.

			M2	M4	M6
Stress (MPa)	Piezo1	@ 50 μT	-2.7	-5.75	-5.67
		@ 100 μT	-6.38	-9.91	-10.79
		@ 300 μT	-13.68	-21.38	-28.52
	Piezo2	@ 50 μT	1.91	2.93	2.15
		@ 100 μT	3.96	5.04	4.36
		@ 300 μT	9.62	10.67	10.2
Strain (ppm)	Piezo1	@ 50 μT	-31.27	-69.64	-65.78
		@ 100 μT	-73.9	-118.05	-127.93
		@ 300 μT	-164.59	-258.91	-339.1
	Piezo2	@ 50 μT	20.9	32.87	25.82
		@ 100 μT	48	55.76	47.6
		@ 300 μT	96.43	122.17	126.87
Piezo potential (V)	Piezo1	@ 50 μT	3.39	7.11	6.89
		@ 100 μT	7.76	12.41	13.18
		@ 300 μT	17.09	26.87	34.91
	Piezo2	@ 50 μT	2.37	3.8	2.97
		@ 100 μT	5.35	6.59	5.69
		@ 300 μT	11.79	14.30	15.1

S3. Modeling: effect of magnetoelectric (ME) coupling on voltage output

The ME coupled MME generator is modeled as a cantilever type beam with a tip mass. Although the width of the cantilever is longer than its length, the dominant vibration mode of the structure is the first mode corresponding to that of typical cantilever beams. The difference between the three generators (M2, M4, and M6) under study are primarily in the number of magnetostrictive layers and the weight of the tip mass. As a resonance frequency of 60 Hz is desired for all generators, the tip mass is tuned to achieve a constant resonance frequency at 60 Hz. The number of magnetostrictive layers in the three generators M2, M4 and M6 are 2, 4, and 6, respectively. The bending moment in the beam is derived to be applied to the composite beam consisting of the piezoelectric and magnetostrictive metglas layers.[2] The bending moment is then substituted in the force balance equations to obtain the governing equations of the motion of the cantilever beam.[3] The piezoelectric coupling coefficient, G, is derived from the bending moment, shape function φ for the beam, and force balance in the case of asymmetric beam. Let the beam has a width denoted by b, piezoelectric layers with an equivalent piezoelectric stress coupling constant e_{31}, and the thickness of layer denoted by t_i. The coupling coefficient, G, for the harvesters under study can be obtained from the following expression.

$$G = \frac{e_{31}\, b}{2}\left(\sum_{i=k}^{2k-2} t_i + \frac{t_{k-1} + t_{2\,k-1}}{2}\right)\varphi'|_L \tag{S1}$$

where, k takes the values 4, 6 and 8 for the M2, M4 and M6 generators, respectively. It can be observed that the coefficient, G, is proportional to the slope of the shape function, L, evaluated at the tip of the beam. The excitation to the ME coupled MME generator is due to the magnetic torque from the magnet tip mass and the magnetostriction from the magnetostrictive layers. The excitation force from the magnet is caused by the torque of the magnet in the oscillating magnetic field.[4] However, the magnetostriction in the respective magnetostrictive layers results in the bending moment causing the beam to deflect.[5] The excitation force due to magnetostriction, F_{ms}, is given as

$$F_{ms} = \sum_{i=1}^{n} e_{31mi} b\, t_i \left(\sum_{k=1}^{i-1} t_k + \frac{t_i}{2} - \bar{z}\right)\varphi'|_L H_1 \tag{S2}$$

where, e_{31mi} is the magnetostrictive stress constant of the i^{th} layer, H_1 is the external magnetic field strength, $\bar{z}$ is the height of the neutral axis, respectively. The total number of layers including the passive adhesive and piezoelectric layers is denoted by n. However, only the magnetostrictive layers contribute to the bending force, while the passive non-magnetic layers do not produce the bending moment. Hence, in the case of M2, i takes the values of 1 and 5. Similarly, the active layers in the case of M4 are 1, 3, 7 and 9, and in the case of M6, i takes the values 1, 3, 5, 9, 11 and 13. Unlike the coupling coefficient, G, it can be observed that the force of magnetostriction depends on the neutral axis height. In addition to the force given by eq. (S2), a force due to the magnetic tip mass acts on the generator.[5] The generator was designed to resonate at the same frequency with either a magnetic or non-magnetic tip mass.

Table S4. The attributes and simulation results for the three ME coupled MME generators – M2, M4 and M6.

Parameter	**M2**	**M4**	**M6**
Total number of PZT layers	2	2	2
Total number of Metglas layers	2	4	6
Magnetic tip mass (g)	10.9	17.9	24.4
Flexural rigidity (mNm^2)	6.97	12.36	18.48
Neutral layer height (μm)	166.9	196.2	218.3
Height of bottom PZT (μm)	165	199	226
Coupling coefficient, G (mN/V)	1.999	2.289	2.622
Magnetic Force per oersted (mN/Oe)	8.427	13.408	18.807
Magnetostrictive Force per oersted (mN/Oe)	1.306	2.355	3.347

The attributes for the three generators are listed in Table S4. It can be observed from the table that the coupling coefficient is 31% higher in M6 than that in M2 although only two piezoelectric layers are used in all three generators. It can be seen that the magnetic force per oersted is proportional to the magnet tip mass. The neutral axis is 2.8 μm and 7.7 μm below the top surface of the bottom piezoelectric layer in M4 and M6, respectively. The voltage generated by the ME coupled MME generators for four levels of magnetic field strength, 50, 100, 300 and 500 μT as a function of load resistance are evaluated. As shown in Fig. S13, the simulation and experimental results match within a 10% error range for the open circuit voltage outputs. The output voltages of M6 generator in high magnetic fields (300 and 500 μT) are greater than the other two as the magnetic force due to the heavier magnetic mass and the stronger magnetostriction. However, the M4 generator shows better output in the low magnetic fields (≤100 μT). As the difference between the modeled and experimental results is less than 10%, the proposed approach can be used to estimate the performance of the MME generators excluding the contribution of the ME coupling. The voltage output from the MME generators with only contribution of the magnetic torque from the magnet tip mass is shown in Fig. S13c, f, and i. The results indicate that the output voltage of the ME coupled MME generator is higher than the MME generator, and the bending moment from the ME coupling enhances the output voltage by 15.5%, 17.6%, and 17.8% in the M2, M4, and M6 generator, respectively (Fig. S14).

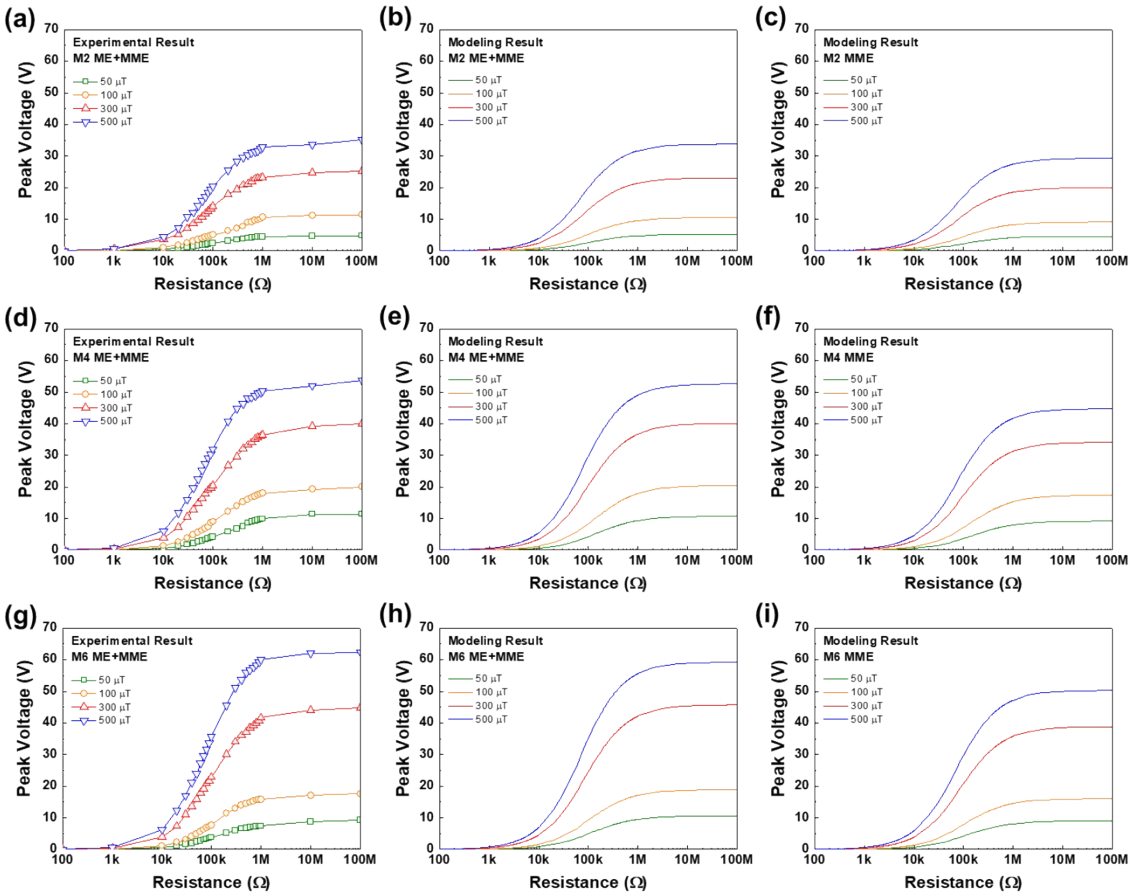

Fig. S13. Measured and modeled output voltages as a function of load resistance and applied AC magnetic field. (a) Measured output voltage from M2 ME coupled MME (b) Modeled output voltage of M2 ME coupled MME generator. (c) Modeled output voltage of M2 MME generator. (d) Measured output voltage from M4 ME coupled MME (e) Modeled output voltage of M4 ME coupled MME generator. (f) Modeled output voltage of M4 MME generator. (g) Measured output voltage from M6 ME coupled MME (h) Modeled output voltage of M6 ME coupled MME generator. (i) Modeled output voltage of M6 MME generator.

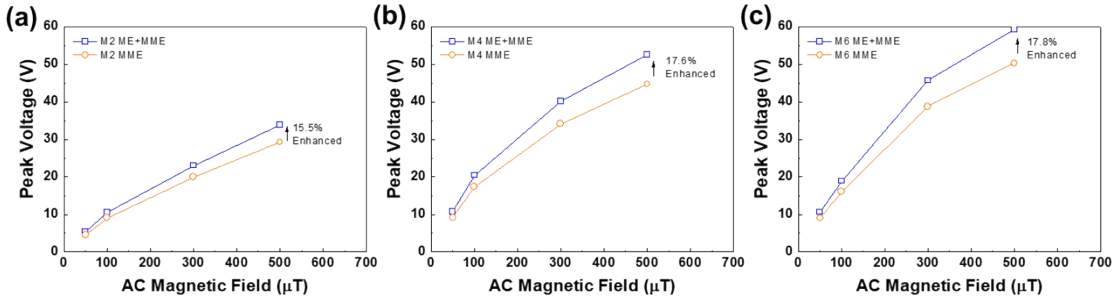

Fig. S14. Modeled open circuit voltage output of the ME coupled MME and MME generators as a function of applied AC magnetic field. (a) M2 (b) M4 (c) M6.

S4. Power output performance

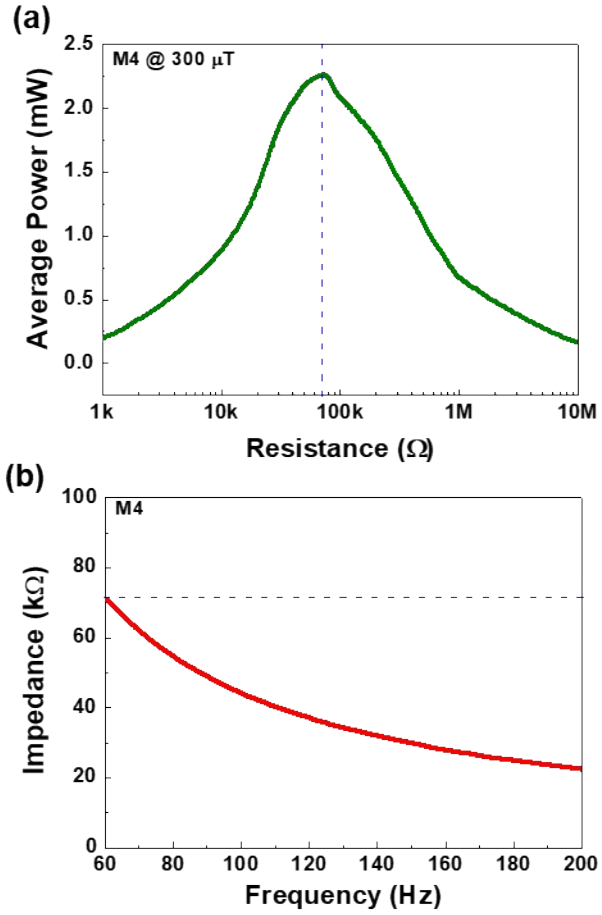

Fig. S15. (a) Average power output of M4 generator under 300 μT AC magnetic field. (b) Impedance of the M4 generator as a function of frequency.

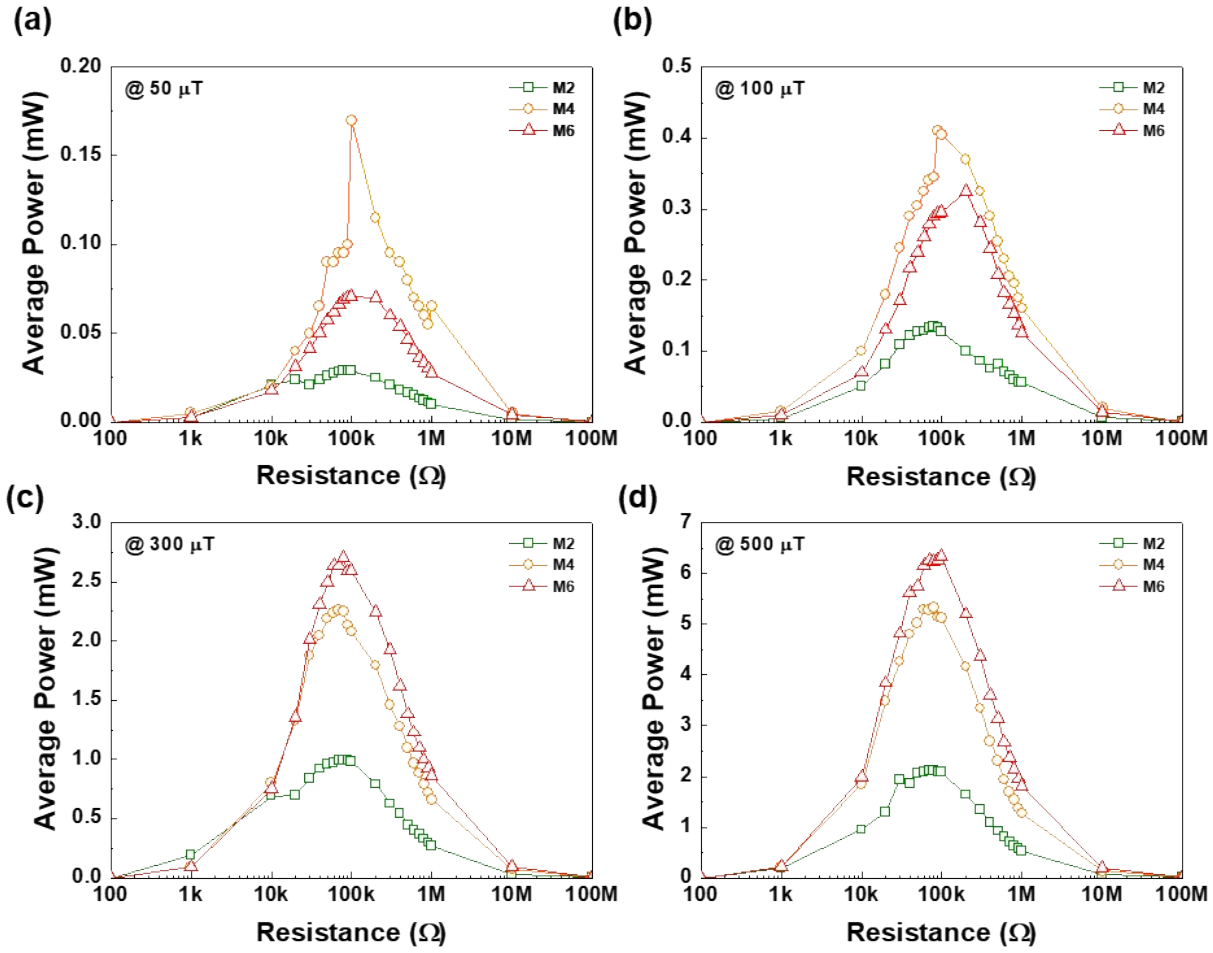

Fig. S16. Average power of the ME coupled MME generators as a function of load resistance under (a) 50 µT (b) 100 µT (c) 300 µT (d) 500 µT.

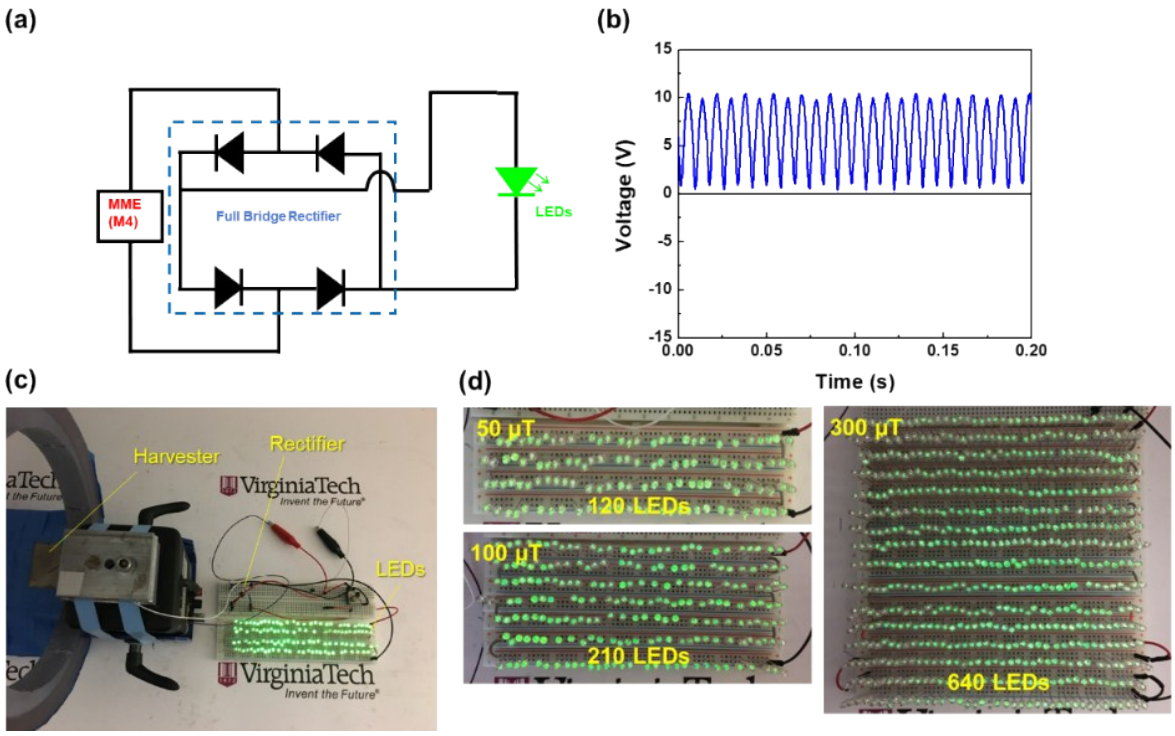

Fig. S17. Powering LED arrays. (a) Electric circuit design for powering LED arrays. (b) Rectified voltage waveform generated from M4 generator under 50 μT. (c) Experimental setup (d) The M4 generator turns on 120, 210, and 640 LEDs under 50 μT, 100 μT, and 300 μT. The LEDs are continuously lighted without charging a capacitor.

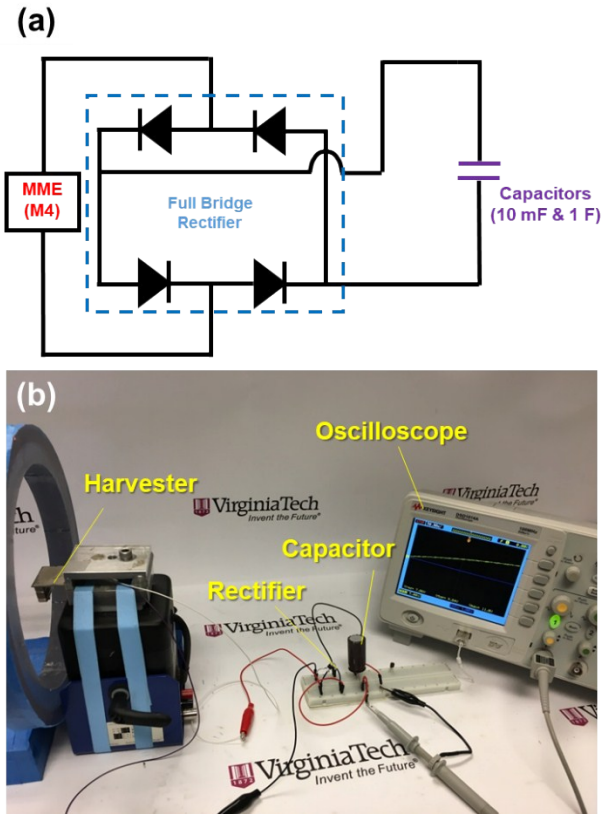

Fig. S18. (a) Electric circuit design for charging capacitors. (b) Experimental setup.

S5. Energy harvesting from ambient stray magnetic fields

Table S5. The stray magnetic field strength in common areas around infrastructure. Note that the magnetic field strength is inversely proportional to the distance squared ($H \propto 1/d^2$).[6]

	Distance from source					Distance from source			
	15 cm	30 cm	60 cm	120 cm		15 cm	30 cm	60 cm	120 cm
Office					**Workshop**				
Air Cleaners	11-25	2-5	0.3-0.8	0-0.2	Battery Chargers	0.3-5	0.2-0.4	-	-
Copy Machines	0.4-20	0.2-4	0.1-1.3	0-0.4	Drill	10-20	2-4	0.3-0.6	-
Fax Machines	0.4-0.9	0-0.2	-	-	Power Saws	5-100	0.9-30	0.1-4	0-4
Fluorescent Lights	2-10	0-3	0-0.8	0-0.4	**Living Room**				
Bathroom					Ceiling Fans	0-5	0-0.6	0-0.1	-
Hair Dryers	0.1-70	0-7	0-1	0-0.1	Window Air Conditioners	0-2	0-0.6	0-0.4	
Electric Shavers	0.4-60	0-10	0-1	0-0.1	TV	0-2	0-0.8	0-0.4	
Kitchen					**Bedroom**				
Blenders	3-10	0.5-2	0-0.3	-	Digital Clock	-	0-0.8	0-0.2	0-0.1
Can Openers	50-150	4-30	0.3-30	0-0.4	Analog Clocks	-	0.1-3	0-0.5	0-0.3
Coffee Makers	0.4-10	0-0.1	-	-	Baby Monitor	0.4-1.5	0-0.2	-	-
Dishwashers	1-10	0.6-3	0.2-0.7	0-0.1	**Laundry/Utility**				
Food Processors	2-13	0.5-2	0-0.3	-	Electric clothes Dryers	0.2-1	0-0.3	-	-
Refrigerators	0-4	0-2	0-1	0-1	Washing Machines	0.4-10	0.1-3	0-0.6	-
Electric Range	2-20	0-3	0-0.9	0-0.6	Irons	0.6-2	0.1-0.3	-	-
Microwave Ovens	10-30	0.1-20	0.1-3	0.1-2	Portable heaters	0.5-15	0.1-40	0-0.8	0-0.1
Mixers	3-60	0.5-10	0-1	-	Vacuum Cleaners	10-70	2-20	0.4-5	0-1

Unit: μT

S6. Layered configuration of MME generators

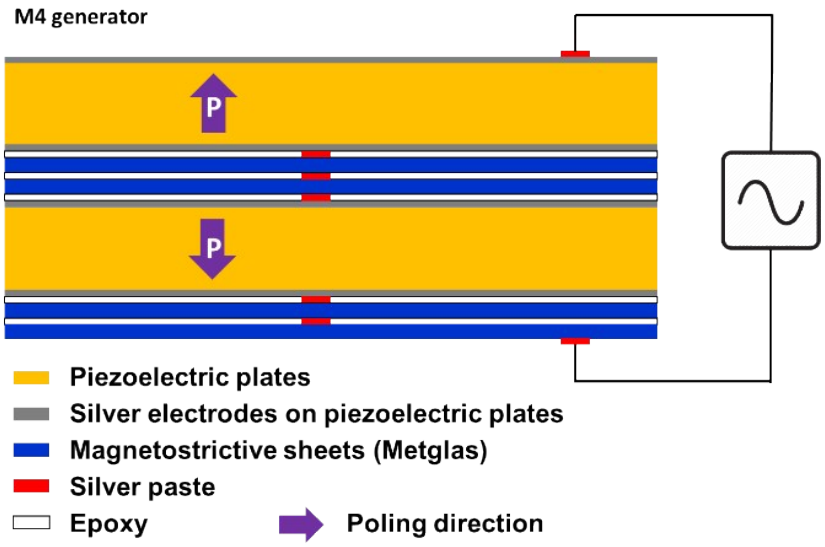

Fig. S19. Schematic description of layered configuration of MME generator.

In order to fabricate the MME generators, 127 μm-thick piezoelectric plates (PSI-5A4E, Piezo System, Inc.) were diced to a dimension of 31 cm × 36 cm by using dicing saw. 23 μm-thick magnetostrictive sheets (2605SA, Metglas) were diced using metal trimmer to have the same size as piezoelectric plates. The piezoelectric plates and magnetostrictive sheets were laminated using epoxy (DP-460, 3M). Small amount of epoxy was applied on the surface of piezoelectric and magnetostrictive layers and dried for 24 h at R.T under heavy load (~5 kg), resulting in a thin epoxy thickness of around 10 μm. To generate high voltage output, the piezoelectric plates are electrically connected in series with opposite poling direction as shown in Fig. S18. Note that total piezoelectric potential generated from the piezoelectric plates can be nearly canceled if the piezoelectric plates are laminated with the same poling direction, as the applied stress on each piezoelectric plate has opposite value under the bending motion as shown in Fig. 2. To demonstrate the series connection between the piezoelectric plates, all the piezoelectric and magnetostrictive layers are electrically connected using silver paste (Leitsilber 200 Silver Paint, Ted Pella) as shown in Fig S19 (red color). To acquire power output from the device, electric wires were connected on both sides of the device using silver paste.

References

1. K. H. Cho, C. S. Park and S. Priya, *Appl. Phys. Lett.*, 2010, **97**, 182902.
2. A. Erturk and D. J. Inman, *Piezoelectric energy harvesting*, Wiley, Chichester, 2011.
3. R. Sriramdas, S. Chiplunkar, R. M. Cuduvally and R. Pratap, *IEEE Sens. J.*, 2015, **15**, 3338-3348.
4. V. Annapureddy, S.-M. Na, G.-T. Hwang, M. G. Kang, R. Sriramdas, H. Palneedi, W.-H. Yoon, B.-D. Hahn, J.-W. Kim and C.-W. Ahn, *Energy Environ. Sci.*, 2018.
5. M. G. Kang, R. Sriramdas, H. Lee, J. Chun, D. Maurya, G. T. Hwang, J. Ryu and S. Priya, *Adv. Energy Mater.*, 2018, **8**, 1703313.
6. *EMF Electric and Magnetic Fields Associated with the Use of Electric Power*, National Institute of Environmental Health Sciences and National Institutes of Health, 2002.